IEEE Access
Multidisciplinary | Rapid Review | Open Access Journal

SPECIAL SECTION ON ENERGY HARVESTING TECHNOLOGIES FOR WEARABLE AND IMPLANTABLE DEVICES

Received October 30, 2020, accepted December 5, 2020, date of publication January 8, 2021, date of current version February 5, 2021.

Digital Object Identifier 10.1109/ACCESS.2021.3050431

Simulation of Crystalline Silicon Photovoltaic Cells for Wearable Applications

JINWEI ZHAO[1,2], (Graduate Student Member, IEEE), ZENGYI XU[1], MAN-KAY LAW[2], (Senior Member, IEEE), HADI HEIDARI[1], (Senior Member, IEEE), SAMEH O. ABDELLATIF[3], (Senior Member, IEEE), MUHAMMAD ALI IMRAN[1], (Senior Member, IEEE), AND RAMI GHANNAM[1], (Senior Member, IEEE)

[1]James Watt School of Engineering, University of Glasgow, Glasgow G12 8QQ, U.K.
[2]State Key Laboratory of Analog and Mixed-Signal VLSI, AMSV, University of Macau, Macau 999078, China
[3]Electrical Engineering Department, The British University in Egypt, Cairo 11837, Egypt

Corresponding author: Rami Ghannam (rami.ghannam@glasgow.ac.uk)

This work was supported by the UK's Engineering and Physical Sciences Research Council (EPSRC) under Grant EP/R511705/1.

ABSTRACT Advancements in the semiconductor industry have enabled wearable devices to be used for a wide range of applications, including personalised healthcare. Novel energy harvesting technologies are therefore necessary to ensure that these devices can be used without interruption. Crystalline silicon photovoltaic (PV) cells provide high energy density to electronic loads. However, the optimization of these cells is a complex task since their optical performance is coupled to the surroundings, while their electrical performance is influenced by the intrinsic PV characteristics and parasitic losses. Without doubt, simulation tools provide the necessary insight to PV cell performance before device fabrication takes place. However, the majority of these tools require expensive licensing fees. Thus, the aim of this article is to review the range of non-commercial PV simulation tools that can be used for wearable applications. We provide a detailed procedure for device modelling and compare the performance of these tools with previously published experimental data. According to our investigations, non-commercial 3D tools such as PC3D provide accurate simulation results that are only $\approx 1.7\%$ different from their commercial counterpart.

INDEX TERMS Energy harvesting, photovoltaics, simulation, wearables.

I. INTRODUCTION

According to the late Nobel laureate, Prof. Richard Smalley, ''energy is the single most important challenge facing humanity today'' [1]. Not only can solar energy help in the democratization of energy, it also has the potential to profoundly enhance the operation of wearable and implantable devices [2], [3]. Such devices primarily rely on rechargeable batteries for satisfying their energy needs. However, since photovoltaic (PV) technology is a mature and reliable method for converting the Sun's vast energy into electricity, innovation in developing new materials and solar cell architectures is becoming more important to increase the penetration of PV technologies in wearable applications.

A PV cell is a basic device that converts the Sun's energy into electricity. Currently, a wide variety of PV cells exist, which range from expensive multi-junction semiconductor cells to lower cost non-crystalline cells. In fact, nearly 90% of today's PV cells are based on crystalline silicon materials and innovations in hybrid as well as non-crystalline PV cells are promising improved efficiency and lower cost. However, expensive laboratory facilities and equipment are often required for the fabrication and characterisation of these cells, which may hinder further research progress in PV cell development. Furthermore, the insight that comes from simulations helps designers understand how PV cells perform prior to testing, which enables them to make the right product design decisions. Consequently, we aim to review the range of experimentally verified multidimensional simulation tools that can be used for designing solar cells. These tools allow researchers to design and numerically investigate the next generation of PV cells before fabrication takes place.

The literature provides a wealth of tools for numerically simulating PV cells [4]. The earliest simulations involved

The associate editor coordinating the review of this manuscript and approving it for publication was Wei E. I. Sha.

solving a set of ''continuum'' partial differential equations, commonly known as the semiconductor equations [5]. Thanks to early efforts at Bell Labs in the 1960s, computer simulations demonstrated that PV cell efficiencies can reach 19% [6], [7]. Improvements in computers enabled these simulations to be performed on personal computers (PCs). Gray and Basore from Purdue University were best known for initiating these modelling efforts during the 1980s and early 1990s with their one-dimensional (1D) simulations programme called PC1D, which solved the semiconductor equations using the finite element method [8]. Later, a more advanced simulation tool called 'A Device Emulation Program and Toolbox' (ADEPT) was developed, which enabled two-dimensional (2D) and three-dimensional (3D) simulations to be performed on crystalline-based PV cells [9]. Currently, Sentaurus Device is the latest commercial tool for simulating PV cells in 2D and 3D from Synopsis [10]. For example, the Atwater group in Caltech used this software to characterize the performance of nanowire silicon solar cells [11].

As previously mentioned, crystalline silicon-based solar cells dominate the PV market [10]. Further penetration of solar energy solutions in the market relies on developing lower cost cells and improving their efficiency. For example, increasing the efficiency of solar cells requires innovations in light trapping and in creating antireflection coatings [12]–[14]. However, enhancing the performance of crystalline solar cells is a non-trivial and complex task, since performance relies on ambient conditions, recombination within the semiconductor and various parasitic losses [10].

To predict the performance of solar cells, the finite-element-method (FEM) has often been used for solving the semiconductor equations describing the electrical carrier properties of solar cells in 1D, 2D or 3D [10]. In the 1D and 2D models, carrier generation and optical absorption are rarely analyzed thoroughly, and only low-dimensional approximations are applied [15]. Since 1D FEM simulations often use the Beer-Lambert method to calculate carrier transport, 1D tools can be used to simulate basic cells without features in the direction parallel to the pn-junction [16]. Compared with the optical approximations in 1D modelling, the electromagnetic (EM) response is calculated using the Jones matrix method in 2D and 3D, which provides more accurate optical analysis [15].

According to the literature, 3D software tools enable accurate simulations that agree with experiments, since parasitic losses can be included. Some of these parasitic losses can be considered using the solar cell's equivalent electrical circuit and its subsequent current-voltage (IV) response equation [15]. These losses can be defined in terms of the equivalent 'series' and 'shunt' resistances.

Nevertheless, the majority of these software tools require expensive licensing fees. Thus, we will review the range of free software tools for simulating PV cells. We will discuss the merits and limitations of these tools. Moreover, we will provide a step-by-step demonstration of how to simulate a simple p-i-n solar cell using a commercial multiphysics FEM tool. Comparisons between the simulations tools will also be provided. Towards the end of the article, we will provide recommendations, conclusions and suggestions for further work.

II. STATE OF THE ART

The earliest PV FEM modelling tool for solar cells was PC1D, as shown from the timeline in Fig. 1. Moreover, a list of free PV modelling tools is shown in TABLE 1.

For example, PC1D and PC3D are two non-commercial tools for 1D and 3D simulations. In the literature, PC1D was previously used to optimise the efficiency of a monocrystalline silicon solar cell with an efficiency of 20.35% [17]. Similarly, due to its 3D modelling capabilities, PC3D was used to accurately simulate the optical properties of light interacting with the PV cell's textured surface as well as its top interdigitated electrode structure [18].

General-Purpose Photovoltaic Device Model (GPVDM) is another semiconductor simulator that enables users to simulate emerging PV cells, such as perovskite cells. For example, it was used to investigate the performance of perovskite PV cells when the active layer thickness and temperature were varied [19]. This tool also provides a 3D graphical representation of a PV cell, but only solves the semiconductor equations in 1D. It has an intuitive output interface that enables users to obtain both electrical and optical PV data, such as the photo absorption rate and the generation rate at different regions within the thickness of the device.

Moreover, Analysis of Microelectronic and Photonic Structures (AMPS) is another free 1D multipurpose simulations tool, which has been used to investigate the effect of varying the absorber layer thickness in Gallium Selenide (CIGS) PV cells for a range from 300 *nm* to 3000 *nm* [20]. It has a library of monocrystalline, polycrystalline and amorphous materials. It can produce Current Density versus Voltage (JV) characteristic curves as well as the quantum efficiency. However, the tool can only be installed on the Win XP platform, since its developers do not support newer operating systems nor platforms.

Furthermore, Solar Cell Capacitance Simulator 1D (SCAPS-1D) has been used for modelling polycrystalline Si PV cells [21], perovskite-based PV cells [22] and thin film PV cells based on Cadmium Telluride (CdTe) [23] and Copper Indium Gallium Selenide (CIGS) [24].

Automat for Simulation of Hetero-structures (AFORS-HET) is another free simulator used to model an arbitrary 1D sequence semiconductor interface [25]. It has been used to simulate heterojunction PV cells [26]. It can produce both electrical and optical PV data. AFORS-HET can also simulate materials with graded bandgaps as well as carrier transport across the various interfaces [27]. However, it is not capable of simulating high dimensional models of solar cells.

We will compare the performance of these non-commercial tools with COMSOL, which is a commercial software

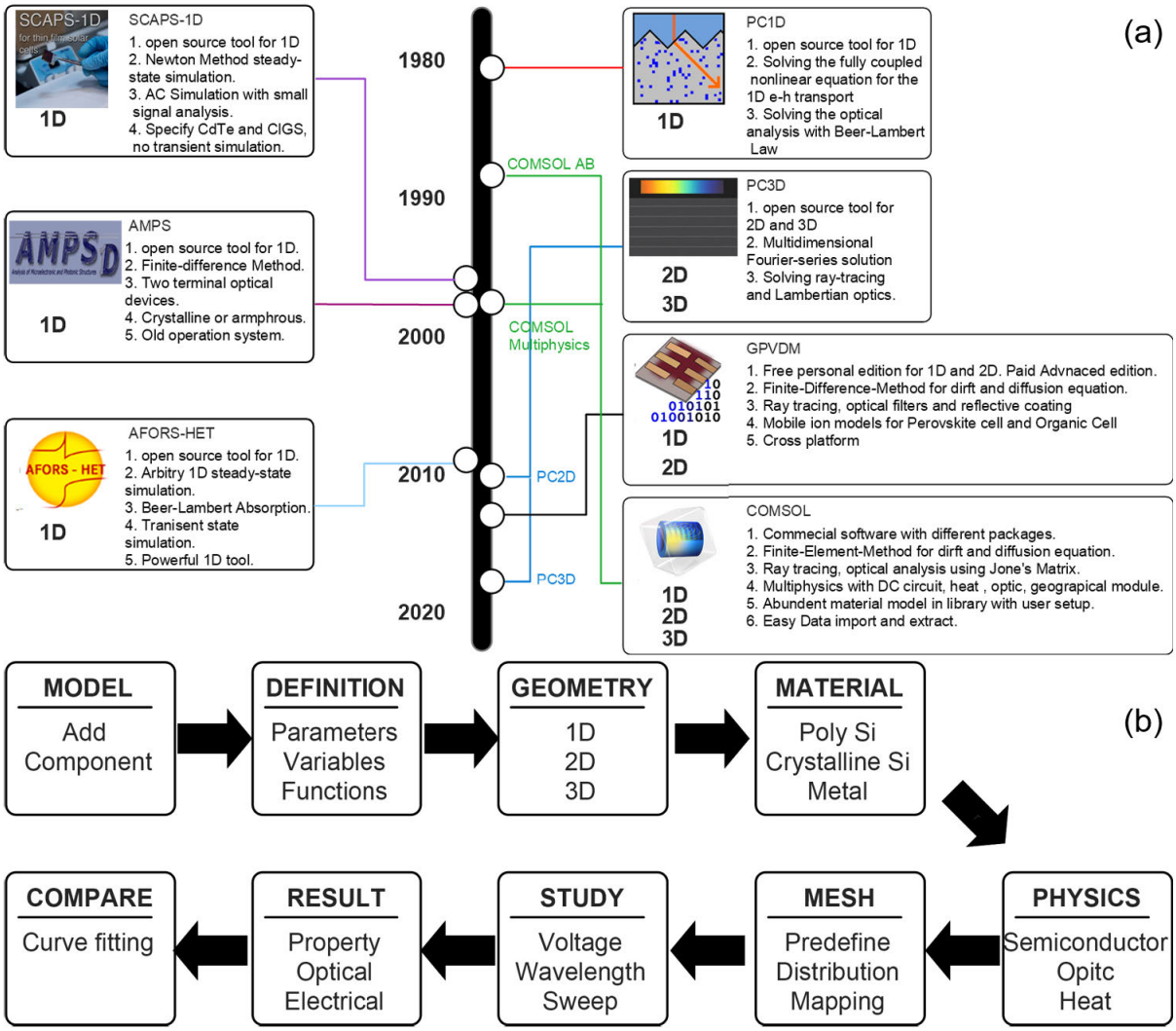

FIGURE 1. (a) Timeline showing the development of four different PV cell simulation tools: PC1D, PC3D, GPVDM and COMSOL. A comparison between their main features is also shown. (b) Diagram showing the modelling workflow in COMSOL FEM simulation. Briefly, the tool enables solar cell performance to be predicted by defining the material parameters, geometry, meshing model and other numerical simulation properties.

program that solves the semiconductor partial differential equation (PDEs) in 1D, 2D and 3D. In addition to its higher dimensional modelling capabilities, COMSOL has an intuitive and easy to use graphical user interface that enables users to simulate different domains and boundary conditions. It has been previously used for simulating the performance of implantable PV cells [2]. Compared with COMSOL, these non commercial tools have a smaller file size and are capable of solving the semiconductor equations in 1D and 3D.

III. METHODOLOGY

The following simulation platforms were used during our investigations: COMSOL Multiphysics 5.4.0.388 with the Semiconductor and Waveoptic modules, PC1D v5.9, PC3D v1.7 and AFORS-HET v2.5. The simulations were performed on a computer with an Intel Core i5-6300U processor (2.40 GHz), 4 GB RAM and a Windows 10 64-bit operating system.

A. DEFINITION AND SETUP

Initially, the parameters, variables and functions were set up in different scenarios, light intensities and device properties. The parameters, functions and variables for the FEM simulation are summarized in TABLE 2. At first, the electrical properties of silicon were defined, which included the intrinsic doping concentration [32], relative permeability [32], electron affinity [32], bandgap [32], density of states [28] and carrier mobility [31].

The density of states and carrier mobility functions are shown in Fig. 2(a) and 2(b). The recombination losses will be determined by the recombination coefficients, such as the Auger coefficient, Radiative coefficient and Shockley-Read-Hall coefficient, which are shown in Fig. 2(c) and 2(d), as well as TABLE 2.

The absorption of light and generation of an electron-hole pair is fundamental to PV cell operation. In this process, the energy of a photon is initially converted to electrical

TABLE 1. Comparison Between Different Simulation Tools.

Software	Dimension	Mathematical solver 5	Focused Theme	Modelling Types
COMSOL	1D/2D/3D	Finite Element Method	General physical theme Organic device	Multiphysics
GPVDM	1D	1D Layer, Finite Deference Method	Crystalline/Amorphous silicon device CIGS solar cells	Semiconductor and electrostatic
PC1D	1D	1D Layer, Newton method	General photovoltaic device	Semiconductor and electrostatic
PC3D	1D/3D	1D/3D Layer, 3D Fourier-series solutions	General photovoltaic device	Semiconductor and electrostatic
AMPS	1D	1D Layer, finite differences (Newton Raphson iteration)	Crystalline/Amorphous silicon device	Semiconductor and electrostatic
SCAPS-1D	1D	1D Layer, Newton method	Poly-crystalline thin film based on CdTe and CIGS	Semiconductor and electrostatic
AFORS-HET	1D	1D layer, Finite difference	Arbitrary semiconductor layer	Semiconductor and electrostatic

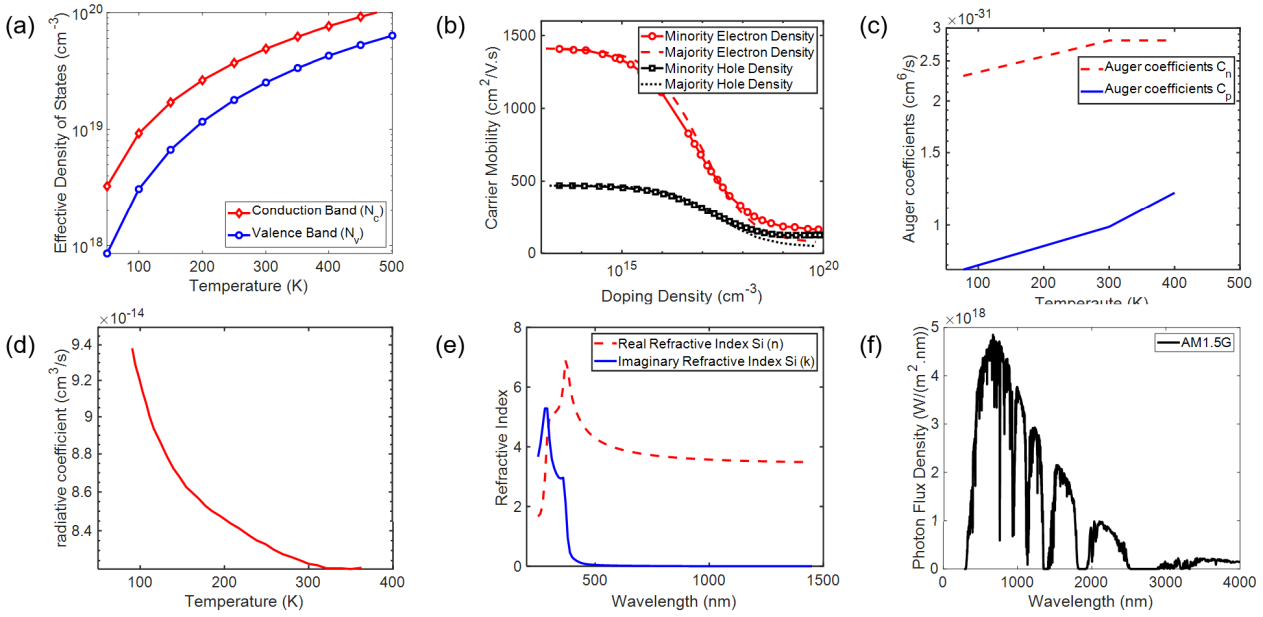

FIGURE 2. (a) Density of states model from Couderc *et al.* 2014 [28]. (b) Carrier mobility parameterization from Klaassen *et al.* 1987 [10]. (c) Auger coefficients of Dziewior and Schmid, which were obtained from P. Altermatt *et al.* 2011 [10]. (d) Radiative recombination coefficient from Nguyen *et al.* 2014 [29]. (e) Refractive index of crystalline Silicon from Aspnes *et al.* 1983 [30]. (f) Photon flux density of AM1.5G spectrum from Nguyen *et al.* 2014 [29].

energy through the creation of an electron-hole pair [4]. The refractive index of silicon was used to analyse the amount of light absorbed or penetrated in the PV cell, as shown in Fig. 2(e).

Moreover, for simulating the performance of PV cells, the AM1.5G global irradiance spectrum was used, where a power density of 1000 W/cm^2 was assumed. The photon flux spectrum shown in Fig. 2(f) was used to set up the generation rate [29]. Unless otherwise stated, an ambient temperature of 300 K was used [32].

B. GEOMETRY DESIGN

Simulating an ideal p-i-n junction diode requires a uniform doping profile in each region. In our simulations, we have defined the different layers as heavy n-type doped (N+), light p-type doped (P-) and heavy p-type doped (P+). The length of these layers was L_{p+}, L_{N+}, and L_{P-}. The device properties and parameters are summarised in TABLE 3. We used these parameters to compare the performance of our simulations tools with experimental data from two different sources [33] and [34].

In our simulations, light penetrates from the bottom of the cell with an incident angle of zero, as shown in figure 3. Therefore, the front surface of the cell was located at $y = 0$. Moreover, two metal contact were added to the front and rear surface of the PV cells.

C. MATERIAL ALIGNMENT

Polycrystalline silicon was used as the device material, with the properties shown in TABLE 2. An 'air' layer was defined on the top and bottom sides of the PV cell with a refractive index of ($N_{Air} = 1.0003$) [35]. Since the doping concentration is different in each layer, parameters such as carrier mobility and recombination coefficient are different. In this

TABLE 2. Summary of Device Simulation Parameters.

Parameters	Function of Value	Description
Equation Iteratively Solved	Poisson's Eq.	X.Li *et al.* 2013 [15]
Free Carrier Statistics	Femi-Dirac	P.P. Altermatt *et al.* 2002 [31]
Temperature	300 K	P.P. Altermatt *et al.* 2011 [10]
Intrinsic Doping Density	$1 \times 10^{10} cm^{-3}$	M.Levinshtein *et al.* 1997 [32]
Relative Permittivity	11.7	M.Levinshtein *et al.* 1997 [32]
Bandgap	1.12 eV	M.Levinshtein *et al.* 1997 [32]
Electron Affinity	4.05 eV	M.Levinshtein *et al.* 1997 [32]
Density of State	Couderc model (Fig.2(a))	Couderc *et al.* 2014 [28]
Carrier Mobility (μ_p, μ_n)	parameterization (Fig.2(b))	P.P.Altermatt *et al.* 2011 [10]
Reconbination Coefficients		
Auger(C_p, C_n)	Dziewior and Schmid (Fig.2(c))	P.P Altermatt *et al.* 2011 [10]
Radiative (B)	Nguyen model (Fig.2.(d))	Nguyen *et al.* 2014 [29]
Optical Parameter		
Refractive Index	Silicon (Fig.2(e))	Aspnes *et al.* 1983 [30]
Optical Spectrum	AM1.5G (Fig.2.(f))	Nguyen *et al.* 2014 [29]

TABLE 3. Devices Properties.

Parameter	[33]	[34]
t	$800\ nm$	$150\ \mu m$
N_{P+}	$1 \times 10^{20}\ cm^{-3}$	$1 \times 10^{19}\ cm^{-3}$
N_{Base}	$1 \times 10^{16}\ cm^{-3}$	$3.5 \times 10^{15}\ cm^{-3}$
N_{N+}	$1 \times 10^{20}\ cm^{-3}$	$1 \times 10^{17}\ cm^{-3}$
L_{p+}	$50\ nm$	$1\ \mu m$
L_{P-}	$500\ nm$	$148.45\ \mu m$
L_{N+}	$250\ nm$	$250\ nm$
I_{rad}	$1000\ W/m^2$	$1000\ W/m^2$
λ	$550\ nm$	$550\ nm$
$\lambda Sweep$	$400 - 1000\ nm$	$400 - 1000\ nm$

case, the materials were set up differently and aligned to specific layers (N+, P− and P+) with different doping concentrations N_{p+}, N_{N+}, and N_{P-}.

D. PHYSICAL MODEL DESCRIPTION

To analyze carrier transport across the heterojunction interfaces, the semiconductor module enables important semiconductor function definition, such as doping, generation, recombination, trap density and space charge density. On the other hand, PC1D, GPVDM and AFORS-HET enable users to customize the doping concentration and diffusion length, while PC3D enables users to define the doping concentration by changing the sheet resistance of each layer. The equations solved by the simulations programs are: [5], [10], [15]:

$$\Delta\left[-D_n\Delta n + n\mu_n\left(\Delta\phi + \frac{\Delta\chi}{q} + \frac{kT}{q}\Delta\ln N_c\right)\right] = G(x, y, z, \lambda) - R \quad (1)$$

$$\Delta\left[-D_p\Delta p + p\mu_p\left(\Delta\phi + \frac{\Delta\chi}{q} + \frac{\Delta E_g}{q} - \frac{kT}{q}\Delta\ln N_c\right)\right] = G(x, y, z, \lambda) - R \quad (2)$$

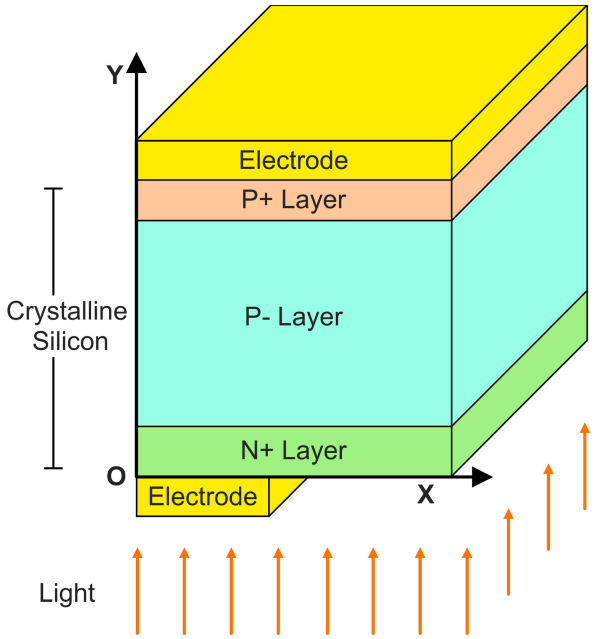

FIGURE 3. Structure and architecture of the experimental PV devices in [33] and [34]. For comparison, we simulated the same structure using COMSOL as well as the non-commercial software programmes.

$$\Delta^2\phi = \frac{q}{\varepsilon_0\varepsilon_r}(n - p - N_D + N_A) \quad (3)$$

where n and p are the electron and hole concentrations, D_n is the electron diffusion coefficient, D_p is the hole diffusion coefficient, μ_n is the electron mobility, μ_p is hole mobility, k is the Boltzmann's constant, $T = 300\ K$ is the operating temperature, q is the electronic charge and ϕ is the electrostatic potential. χ is the electron affinity and E_g is the bandgap. N_c (N_v) is the effective conduction (valence) band density, R is the carrier recombination rate and G is the generation rate. Furthermore, ϵ_0 and ϵ_r are the permittivity of free space and the relative permittivity of crystalline silicon. N_D and N_A are the ionized donor and acceptor concentrations. The recombination consists of the Shockley-Read-Hall, Radiative and Auger recombinations [10]:

$$R = R_{SRH} + R_{rad} + R_{aug} \quad (4)$$

$$R_{SRH} = \frac{np - n_i^2}{\tau_n(p + p_t) + \tau_p(n + n_t)} \quad (5)$$

$$R_{\text{rad}} = B_{\text{rad}}\left(np - n_i^2\right) \quad (6)$$

$$R_{\text{ang}} = \left(C_n n + C_p p\right)\left(np - n_i^2\right) \quad (7)$$

where p_t and n_t are the hole and electron trap concentrations. In fact, highest R_{SRH} are achieved when $n_t = p_t = n_i$. Moreover, B_{rad} is the radiative coefficient, C_n and C_p are the Auger coefficients for electron and holes, τ_p and τ_n are the recombination lifetimes of electrons and holes.

Similarly, the generation rate is expressed in terms of:

$$G = \alpha N_0 e^{-\alpha y} \quad (8)$$

where N_0 is the photon flux at the surface (shown in Fig. 3(f)), α is the absorption coefficient ($\alpha = 4\pi$ Si(k)/λ, where Si(k)

is the imaginary part of refractive index shown in Fig. 2(e)), and y is the distance into the material.

E. OPTICAL CALCULATIONS

To determine the optical characteristics in 2D, the 2×2 Jones Matrix method was used [30]:

$$\begin{bmatrix} E_{Ra} \\ B_{Ra} \end{bmatrix} = \sum_{i=1}^{m} \begin{bmatrix} \cos\varphi_i & \left(\frac{j}{\eta_i}\right)\sin\varphi_i \\ j\eta_i \sin\varphi_i & \cos\varphi_t \end{bmatrix} \begin{bmatrix} 1 \\ \eta_m \end{bmatrix} \quad (9)$$

where δ_i is the wave phase shift ($\delta_i = 2\pi N_i d_i cos\theta i/\lambda$) in the i^{th} layer, N_i is the refractive index, d_i is the thickness of the i^{th} layer, η_i is the pseudo index in i^{th} layer ($\eta_i = N_i cos\theta_i$). E_{Ra} or B_{Ra} is the ratio between the electric and magnetic fields of the transmitted light and incident light. M is the total number of layers. The reflectance (R), absorptance (A) transmittance ($T = 1 - A - R$) of light can be determined using:

$$R = \frac{4\eta_0 \,\mathrm{Re}\,(\eta_m)}{\left(\eta_0 E_{Ra} + B_{B_n}\right)\left(\eta_0 E_{Ra} + B_{Ra}\right)^*} \quad (10)$$

$$A = \frac{4\eta_0 \,\mathrm{Re}\left(E_{Ra} B^*_{Ra} - \eta_m\right)}{\left(\eta_0 E_{Ra} + B_{B_0}\right)\left(\eta_0 E_{Ra} + B_{Ra}\right)^*} \quad (11)$$

1) INITIAL CONDITION SETUP

Initially, we applied the neutral charge condition to setup the doping profile and ohmic contact characteristics for estimating the initial electrostatic potential. The initial doping profiles for p-type (p_{init}) and n-type (n_{init}) doping were defined by applying the neutral charge condition, where $n_{init} - p_{init} - C = 0$ and $n_{init} p_{init} = n_i^2$. These can be described in terms of:

$$n_{init} = \frac{1}{2}\left(\sqrt{C^2 + 4n_i^2} + C\right) \quad (12)$$

$$p_{init} = \frac{1}{2}\left(\sqrt{C^2 + 4n_i^2} - C\right) \quad (13)$$

$$\Phi_{\text{init}} = \frac{kT}{q} \arcsin h \frac{C}{2n_i} \quad (14)$$

This initial electrostatic potential can be estimated for ohmic contacts. It can also predict the initial potential profile and the doping profile in a homojunction.

2) BOUNDARY CONDITIONS

Periodic boundary conditions were used in the transverse directions for both carrier diffusion and electrostatic potential. Along the junction interface, surface recombination conditions were used for the carrier diffusion modules. For the Poisson equations under forward bias, the cathode was grounded and unchanged, but the voltage at the anode was varied from an initial value of zero to the forward bias voltage. In COMSOL and AFORS-HET, the boundary conditions can be customized.

F. ELECTRICAL OUTPUT CHARACTERISTIC

First, the electron current density (J_n), hole current density (J_p) and short-circuit current density (J_{sc}) can be determined using:

$$J_n = -q\mu_n n \nabla\psi - qD_n \nabla n \quad (15)$$

$$J_p = -q\mu_p p \nabla\psi - qD_p \nabla p \quad (16)$$

$$J_{sc} = \iiint \left|J_n(x, y, \lambda) + J_p(x, y, \lambda)\right| dx.dy.d\lambda \quad (17)$$

Considering the parasitic resistances, the output current density of the PV cell can be obtained using:

$$J(V) = -J_0 e^{-\frac{V}{V_T}} + J_{sc} - \frac{V + J(V)R_s}{R_{sh}} \quad (18)$$

where R_s and R_{sh} are the series and shunt parasitic resistances, and V_T is the thermal voltage ($V_T = kT/q$). Since our simulations model is in 2D, R_s can be neglected and R_{sh} can be calculated using the current-voltage (IV) characteristics of the device. The External Quantum Efficiency (EQE) can be determined using:

$$EQE = \frac{hcJ_{sc}}{q\lambda I_{rad}} \quad (19)$$

where h is the Plank constant, c is the speed of light, I_{rad} is the irradiance under AM 1.5G.

G. SEMICONDUCTOR AND SIMULATION SETUP

In PC1D, GPVDM and AFORS-HET, the doping concentration and diffusion length in each semiconductor layer need to be defined. However, in PC3D the setting are different, since the relative doping concentrations need to be converted into a sheet resistance. The doping profile were set according to the parameters given in TABLE 3.

In the PC1D, PC3D, GPVDM and AFORS-HET, only the surface recombination can be customized, while COMSOL enables users to define different types of recombination. Moreover, PC1D, PC3D, GPVDM and AFORS-HET enable users to change the irradiance settings as well as the surface reflection.

In COMSOL, two types of doping profiles can be defined, which are 'gradient' and 'uniform'. To ensure consistency with the non-commercial tools, we have used the 'uniform' doping in PC1D, PC3D, GPVDM and AFORS-HET as well as COMSOL. Then, the generation function was set to excite the electron-hole pairs in the device. Furthermore, in the COMSOL programme three types of recombination were defined by invoking eqs. 4-7.

Since the doping concentration is high in the heavily doped regions (N+ and P+), the bandgap narrowing functionality in COMSOL was used. Next, two metal contacts (Anode and Cathode) were defined to complete the PV cell architecture. Moreover, when selecting a 'Terminal Type', there were four available options in COMSOL, which were Charge, Voltage, Circuit, or Terminated. In this case, we selected 'Voltage'. Finally, for 'Contact Type' we selected 'Ideal Ohmic'. To complete our analysis of these PV cells, we investigated their performance with respect to voltage as well as forward biasing voltage. We therefore varied the voltage between 0 and 0.7 V, whereas the wavelength range was $400\tilde{n}m < \lambda < 1000\ nm$.

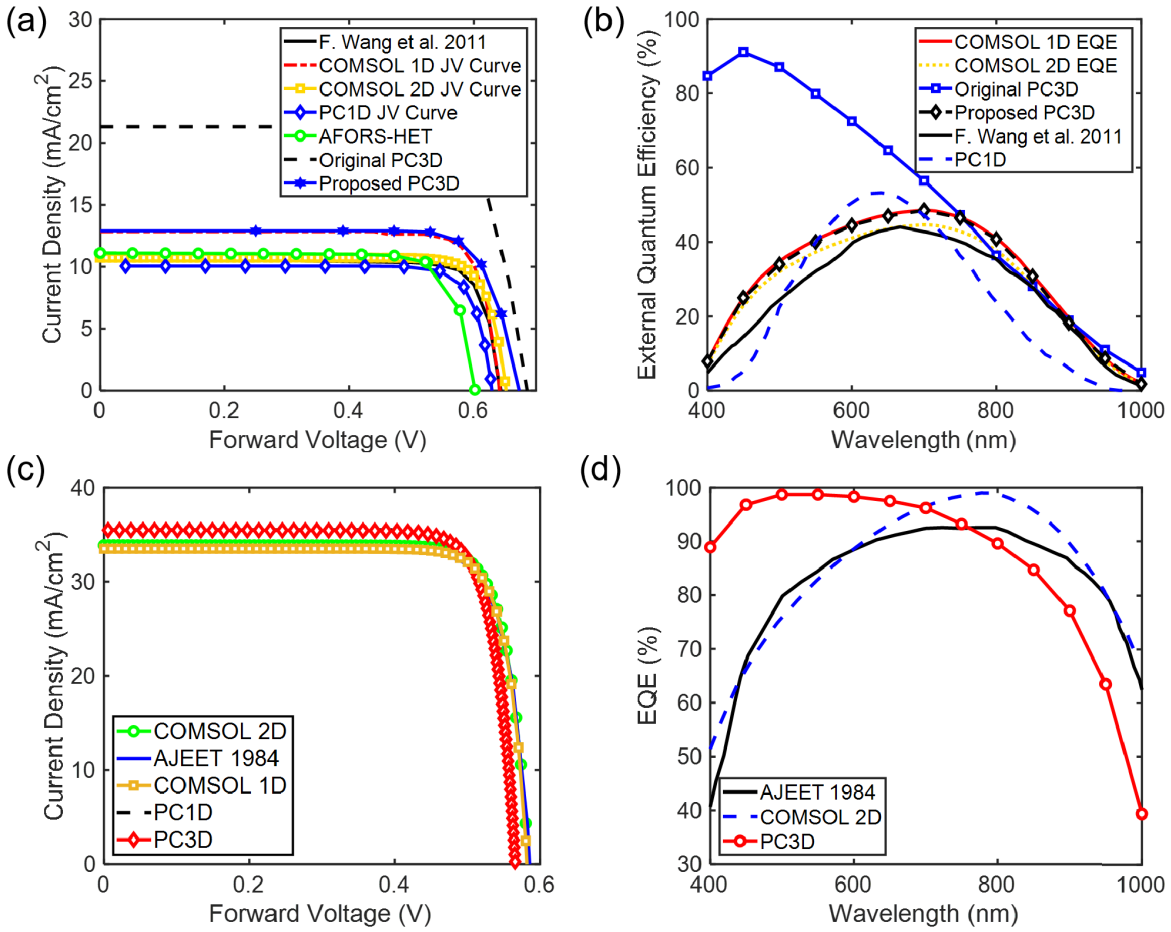

FIGURE 4. (a) Comparison between the simulation results from PC1D, PC3D (original and proposed), COMSOL, AFORS-HET and experimental data from F. Wang *et al.* 2011 [33]. (b) External Quantum Efficiency results from PC1D, PC3D, COMSOL 1D, COMSOL 2D and experimental data from F. Wang *et al.* 2011 [33]. (c) Comparison between simulation results from PC1D, PC3D, COMSOL 2D and experimental data from A. Rohatgi *et al.* 1984 [34]. (d) External Quantum Efficiency results from PC1D, PC3D, COMSOL 2D and experimental data from A. Rohatgi *et al.* 1984 [34].

IV. RESULTS AND DISCUSSION

We compared our simulation results with experimental data from [33], [34], [36]. The PV cell properties were provided in TABLES 2 and 3. As previously mentioned, the modeled solar cell consists of five stacked layers, which are air, a layer of N+ silicon, an intrinsic layer, P+ layer, followed by another layer of air. A comparison between the JV curves for the simulation programmes is shown in Fig. 4. Despite using the parameters, the simulations tools provided different results. We will discuss which tools provided better agreement with experimental data.

Clearly, the simulation results from COMSOL 2D and PC1D are closely matched to experimental data. However, results from COMSOL 1D are different from experimental data. In fact, there is almost a 2 mA/cm^2 difference in J_{sc}), as shown in Fig. 4(a). We believe that this could be attributed to the optical approximation invoked by using the Beer-Lambert Law. Despite the difference in J_{sc}, the V_{oc} data from PC1D as well as COMSOL 1D and 2D all agree with experimental data (0.64 V).

Based on these simulation results, PC1D can be regarded as a reliable software tool that agrees with experiments. This is perhaps why it has been regularly used by the PV industry for decades. With COMSOL 1D and 2D, there are plenty of library resources and multi-physics modules that can facilitate the modelling of different materials and device architectures. Furthermore, numerical solutions to the PV equations were achieved in less than 5 s with COMSOL 1D, while the 2D COMSOL simulations needed $10 - 30$ s.

With AFORS-HET, our PV cell modelling achieved $J_{sc} = 11$ mA/cm^2 and $V_{oc} = 0.6$ V, which compares favourably with experimental as well as the COMSOL data. In fact, AFORS-HET is useful since it allows the user to define different interface materials and boundary conditions. These functionalities are not available in the other surveyed 1D simulation tools.

As shown from Fig. 4(a), PC3D provides slightly different results. Initially, $J_{sc} = 21.3$ mA/cm^2 and $V_{oc} = 0.69$ V. This large difference in results was due to using the default spectral transmission parameters in PC3D, where no reflectance was

assumed. However more accurate results can be obtained by modifying the optical parameters. As previously mentioned, the front spectral reflectance was set to 70% [37] and the back reflectace was set to 50% [38], which enabled the EQE results to match those from COMSOL 1D, as shown in Fig. 4(b). Thus, an improved curve with $J_{sc} = 12.9\ mA/cm^2$ and $V_{oc} = 0.67\ V$ was obtained.

With PC3D, the software can only simulate devices with thicknesses exceeding $1\mu m$. This is an important limitation, especially for wearable PV devices, where thin film materials are now attracting interest. For the sake of comparison, the experimental device in [33] is 20% smaller than this limit, whereby the thickness of the PV cell was 800 nm. Naturally, since the simulated PV cell is thicker than the experimental cell in [33], the $J_{sc} = 12.9\ mA/cm^2$, which is larger than the J_{sc} reported in [33] ($10.5\ mA/cm^2$). Consequently, there is a -22.9% difference between these experimental and simulation J_{sc} results.

Due to this limitation with PC3D, we have also investigated a thicker PV cell with a thickness of 150 μm), as reported in [34]. From our simulation results in PC3D, $J_{sc} = 35.5\ mA/cm^2$, which is much closer to the experimental results mentioned in [34] ($J_{sc} = 36.1\ mA/cm^2$), as can be verified from the results in Fig. 4(c). Therefore, the difference between the experimental and simulation results is now only 1.7%.

As for the External Quantum Efficiency (EQE) results shown in Fig 4(b) and (d), COMSOL shows better agreement with experimental data compared with PC1D and PC3D. The mismatch in results is mainly due to the material and optical properties setup in these programs. For example, in COMSOL three types of recombination can be defined, which are Radiative, Auger and Schockley-Read-Hall recombination. On the other hand, in PC1D and PC3D only surface and bulky recombination can be defined. Furthermore, in PC3D the EQE is usually calculated using the previously mentioned default optical parameters. Including the front and back spectral reflectance leads to better agreement with experimental data, as shown from the 'Proposed PC3D' curve results in figure 4. Consequently, this proves that the PC3D simulation results can be setup to show good agreement with experimental data.

Clearly, COMSOL is a software tool with a vast materials library, great curve fitting features and a multiphysics environment, which produces results that agree with experimental data. It can therefore be used to accurately predict the performance of PV cells for wearable applications, particularly when such cells are exposed to non-uniform lighting conditions. In that case, the 3D PV cell model can be used to investigate the change in irradiance along the horizontal and vertical axes. Secondly, wearable applications require highly flexible devices for improved user comfort. In 3D modelling, it is easier to analyze the stress and pressure inside the device. Eventually, the PV cell semiconductor model in 3D COMSOL can be easily integrated with other multi-physics modules to investigate the impact of heat, pressure and other environmental effects. In this case, PC3D is an alternative and free option that can perform many of COMSOL's simulations, provided that devices are larger than $1\mu m$. This is also especially true if the device properties library is complete, with an ability to modify the optical properties. We can also obtain more accurate results if multi-physics simulations can be involved, where the effects of temperature and stress can be investigated.

V. CONCLUSION

In this article we provided a review of the different non-commercial software tools for simulating PV cells that can be used in wearable applications. In total, we reviewed five different software programmes. We also provided a detailed procedure for simulating a p-i-n solar cell using a set of predefined solar cell parameters. Using these parameters, we subsequently compared these simulation results with a commercial, multiphysics simulations program called COMSOL, which solves the semiconductor equations using the finite element method (FEM). According to our investigations, all simulation tools provided different results. This was due to their differing approaches for solving the semiconductor equations. Nevertheless, we concluded that PC3D is the most accurate non-commercial tool for wearable applications, since their results closely match the data from COMSOL, particularly since the data also agreed with previously published experiments.

REFERENCES

[1] US Senate Committee on Energy and Natural Resources. (2020). *Transcript of the Testimony of Richard E. Smalley to the US Senate Committee on Energy and Natural Resources*. Accessed: Oct. 9, 2020. [Online]. Available: https://www.gpo.gov/fdsys/pkg/CHRG-108shrg95239/html/CHRG-108shrg95239.%htm

[2] J. Zhao, R. Ghannam, M.-K. Law, M. A. Imran, and H. Heidari, "Photovoltaic power harvesting technologies in biomedical implantable devices considering the optimal location," *IEEE J. Electromagn., RF Microw. Med. Biol.*, vol. 4, no. 2, pp. 148–155, Jun. 2020.

[3] J. Zhao, R. Ghannam, K. O. Htet, Y. Liu, M.-K. Law, V. A. Roy, B. Michel, M. A. Imran, and H. Heidari, "Self-powered implantable medical devices: Photovoltaic energy harvesting review," *Adv. Healthcare Mater.*, vol. 9, no. 17, 2020, Art. no. 2000779.

[4] P. Altermatt, *Numerical Simulation of Crystalline Silicon Solar Cells*. Hoboken, NJ, USA: Wiley, 2016, ch. 3.8, pp. 150–159. [Online]. Available: https://onlinelibrary.wiley.com/doi/abs/10.1002/9781118927496.ch15

[5] W. Van Roosbroeck, "Theory of the flow of electrons and holes in germanium and other semiconductors," *Bell Syst. Tech. J.*, vol. 29, no. 4, pp. 560–607, Oct. 1950.

[6] J. G. Fossum, "Computer-aided numerical analysis of silicon solar cells," *Solid-State Electron.*, vol. 19, no. 4, pp. 269–277, Apr. 1976.

[7] J. G. Fossum, "Physical operation of back-surface-field silicon solar cells," *IEEE Trans. Electron Devices*, vol. 24, no. 4, pp. 322–325, Apr. 1977.

[8] P. A. Basore, "Numerical modeling of textured silicon solar cells using PC-1D," *IEEE Trans. Electron Devices*, vol. 37, no. 2, pp. 337–343, Feb. 1990.

[9] J. L. Gray, "ADEPT: A general purpose numerical device simulator for modeling solar cells in one-, two-, and three-dimensions," in *Proc. Conf. Rec. 22nd IEEE Photovoltaic Spec. Conf.*, Oct. 1991, pp. 436–438.

[10] P. P. Altermatt, "Models for numerical device simulations of crystalline silicon solar cells—A review," *J. Comput. Electron.*, vol. 10, no. 3, pp. 314–330, Sep. 2011.

[11] M. D. Kelzenberg, M. C. Putnam, D. B. Turner-Evans, N. S. Lewis, and H. A. Atwater, "Predicted efficiency of Si wire array solar cells," in *Proc. 34th IEEE Photovoltaic Spec. Conf. (PVSC)*, Jun. 2009, pp. 001948–001953.

[12] H. A. Atwater, "Seeing the light in energy use," *Nanophotonics*, vol. 10, no. 1, pp. 115–116, Dec. 2020. [Online]. Available: https://www.degruyter.com/view/journals/nanoph/10/1/article-p115.xml
[13] S. Abdellatif, K. Kirah, R. Ghannam, A. S. G. Khalil, and W. Anis, "Enhancing the absorption capabilities of thin-film solar cells using sandwiched light trapping structures," *Appl. Opt.*, vol. 54, no. 17, pp. 5534–5541, Jun. 2015. [Online]. Available: http://ao.osa.org/abstract.cfm?URI=ao-54-17-5534
[14] S. Abdellatif, R. Ghannam, and A. S. G. Khalil, "Simulating the dispersive behavior of semiconductors using the lorentzian-drude model for photovoltaic devices," *Appl. Opt.*, vol. 53, no. 15, pp. 3294–3300, May 2014. [Online]. Available: http://ao.osa.org/abstract.cfm?URI=ao-53-15-3294
[15] X. Li, N. P. Hylton, V. Giannini, K.-H. Lee, N. J. Ekins-Daukes, and S. A. Maier, "Multi-dimensional modeling of solar cells with electromagnetic and carrier transport calculations," *Prog. Photovoltaics, Res. Appl.*, vol. 21, no. 1, pp. 109–120, Jan. 2013.
[16] J. Nelson, *The Physics of Solar Cells*. London, U.K.: Imperial College Press, 2003.
[17] G. Hashmi, A. R. Akand, M. Hoq, and H. Rahman, "Study of the enhancement of the efficiency of the monocrystalline silicon solar cell by optimizing effective parameters using PC1D simulation," *Silicon*, vol. 10, no. 4, pp. 1653–1660, Jul. 2018.
[18] P. A. Basore, "Efficient computation of multidimensional lambertian optical absorption," *IEEE J. Photovolt.*, vol. 9, no. 1, pp. 106–111, Jan. 2019.
[19] H. Abdulsalam, G. Babaji, and H. T. Abba, "The effect of temperature and active layer thickness on the performance of ch3nh3pbi3 perovskite solar cell: A numerical simulation approach," *J. Found. Appl. Phys.*, vol. 5, no. 2, pp. 141–151, 2018.
[20] J. Ray, C. Panchal, M. Desai, and U. Trivedi, "Simulation of CIGS thin film solar cells using amps-1D," *J. Nano-Electron. Phys.*, vol. 3, no. 1, pp. 747–754, 2011.
[21] M. Burgelman, P. Nollet, and S. Degrave, "Modelling polycrystalline semiconductor solar cells," *Thin Solid Films*, vols. 361–362, pp. 527–532, Feb. 2000.
[22] S. Bansal and P. Aryal, "Evaluation of new materials for electron and hole transport layers in perovskite-based solar cells through SCAPS-1D simulations," in *Proc. IEEE 43rd Photovoltaic Spec. Conf. (PVSC)*, Jun. 2016, pp. 0747–0750.
[23] C.-H. Huang and W.-J. Chuang, "Dependence of performance parameters of CdTe solar cells on semiconductor properties studied by using SCAPS-1D," *Vacuum*, vol. 118, pp. 32–37, Aug. 2015.
[24] M. Mostefaoui, H. Mazari, S. Khelifi, A. Bouraiou, and R. Dabou, "Simulation of high efficiency CIGS solar cells with SCAPS-1D software," *Energy Procedia*, vol. 74, pp. 736–744, Aug. 2015.
[25] A. Froitzheim, R. Stangl, L. Elstner, M. Kriegel, and W. Fuhs, "AFORS-HET: A computer-program for the simulation of heterojunction solar cells to be distributed for public use," in *Proc. 3rd World Conf. Photovoltaic Energy Convers.*, vol. 1, May 2003, pp. 279–282.
[26] M. Ghannam and Y. Abdulraheem, "Electro-physical interpretation of the degradation of the fill factor of silicon heterojunction solar cells due to incomplete hole collection at the a-Si:H/c-Si thermionic emission barrier," *Appl. Sci.*, vol. 8, no. 10, p. 1846, Oct. 2018.
[27] M. Riaz, A. C. Kadhim, S. K. Earles, and A. Azzahrani, "Variation in efficiency with change in band gap and thickness in thin film amorphous silicon tandem heterojunction solar cells with AFORS-HET," *Opt. Exp.*, vol. 26, no. 14, p. A626, 2018.
[28] R. Couderc, M. Amara, and M. Lemiti, "Reassessment of the intrinsic carrier density temperature dependence in crystalline silicon," *J. Appl. Phys.*, vol. 115, no. 9, Mar. 2014, Art. no. 093705, doi: 10.1063/1.4867776.
[29] H. T. Nguyen, S. C. Baker-Finch, and D. Macdonald, "Temperature dependence of the radiative recombination coefficient in crystalline silicon from spectral photoluminescence," *Appl. Phys. Lett.*, vol. 104, no. 11, Mar. 2014, Art. no. 112105.
[30] D. E. Aspnes and A. A. Studna, "Dielectric functions and optical parameters of Si, ge, GaP, GaAs, GaSb, InP, InAs, and InSb from 1.5 to 6.0 eV," *Phys. Rev. B, Condens. Matter*, vol. 27, no. 2, pp. 985–1009, Jan. 1983, doi: 10.1103/PhysRevB.27.985.
[31] P. P. Altermatt, J. O. Schumacher, A. Cuevas, M. J. Kerr, S. W. Glunz, R. R. King, G. Heiser, and A. Schenk, "Numerical modeling of highly doped Si:P emitters based on Fermi–Dirac statistics and self-consistent material parameters," *J. Appl. Phys.*, vol. 92, no. 6, pp. 3187–3197, Sep. 2002.
[32] M. Levinshtein, *Handbook Series on Semiconductor Parameters*, vol. 1. Singapore: World Scientific, 1997.
[33] F. Wang, H. Yu, J. Li, S. Wong, X. W. Sun, X. Wang, and H. Zheng, "Design guideline of high efficiency crystalline Si thin film solar cell with nanohole array textured surface," *J. Appl. Phys.*, vol. 109, no. 8, Apr. 2011, Art. no. 084306.
[34] A. Rohatgi and P. Rai-Choudhury, "Design, fabrication, and analysis of 17-18-percent efficient surface-passivated silicon solar cells," *IEEE Trans. Electron Devices*, vol. 31, no. 5, pp. 596–601, May 1984.
[35] P. E. Ciddor, "Refractive index of air: New equations for the visible and near infrared," *Appl. Opt.*, vol. 35, no. 9, pp. 1566–1573, 1996.
[36] S. M. Wong, H. Y. Yu, Y. Li, J. Li, X. W. Sun, N. Singh, P. G. Q. Lo, and D.-L. Kwong, "Boosting short-circuit current with rationally designed periodic Si nanopillar surface texturing for solar cells," *IEEE Trans. Electron Devices*, vol. 58, no. 9, pp. 3224–3229, Sep. 2011.
[37] J. Humlíček and K. Vojtěchovský, "Infrared optical constants of N-type silicon," *Czechoslovak J. Phys.*, vol. 38, no. 9, pp. 1033–1049, Sep. 1988.
[38] S. Strehlke, S. Bastide, and C. Lévy-Clément, "Optimization of porous silicon reflectance for silicon photovoltaic cells," *Sol. Energy Mater. Sol. Cells*, vol. 58, no. 4, pp. 399–409, Aug. 1999.

JINWEI ZHAO (Graduate Student Member, IEEE) received the B.Eng. degree in electrical and electronics engineering from The University of Edinburgh, in 2016, and the M.Sc. degree in electric power from Newcastle University, U.K., 2017. He is currently pursuing the Ph.D. degree with the University of Glasgow. He participated in the FDCT (The Science and Technology Development Fund) funded project "High Efficiency Energy Harvesting System for Biomedical Devices" and exchanged to the State Key Laboratory of Analog and Mixed-Signal VLSI Group, University of Macau, in 2019. His research interests include energy harvesting, implantable systems, and photovoltaic cells.

ZENGYI XU is currently pursuing the B.Eng. degree in electrical and electronic engineering from the University of Glasgow. In the summer of 2020, he participated in the research project of Energy harvesting at the University of Glasgow. During that research experience, he obtained valuable knowledge of team cooperation and fundamental skills in semiconductor simulation. His current interests include optical communication, photovoltaic device, and light emitting diode.

MAN-KAY LAW (Senior Member, IEEE) received the B.Sc. degree in computer engineering and the Ph.D. degree in electronic and computer engineering from The Hong Kong University of Science and Technology (HKUST), in 2006 and 2011, respectively. In February 2011, he joined as a Visiting Assistant Professor with HKUST. He is currently an Assistant Professor with the State Key Laboratory of Analog and Mixed-Signal VLSI, Faculty of Science and Technology, University of Macau, Macau, China. He has authored or coauthored more than 80 technical publications and six U.S./Chinese patents. He has developed world-leading ultra-low power CMOS temperature/image sensing systems, and fully integrated high efficiency solar/ultrasound energy harvesting solutions for implantable applications. His research interests include the development of ultra-low power CMOS sensing/readout circuits and energy harvesting techniques for wireless and biomedical applications.

He was a member of the Technical Program Committee of International Solid-State Circuit Conference (ISSCC), University Design Contest Co-Chair of Asia and South Pacific Design Automation Conference (ASP-DAC), Asia Symposium on Quality Electronic Design (ASQED), and the Review Committee Member of the IEEE International Symposium on Circuits and Systems (ISCAS), the Biomedical Circuits and Systems Conference (BioCAS), and the International Symposium on Integrated Circuits (ISIC). He serves as a Technical Committee Member for the IEEE CAS committee on Sensory Systems and Biomedical and Life Science Circuits and Systems. He was a co-recipient of the ASQED Best Paper Award, in 2013, the A-SSCC Distinguished Design Award, in 2015, the ASPDAC Best Design Award, in 2016, and the ISSCC Silkroad Award, in 2016. He also received the Macao Science and Technology Invention Award (2nd Class) by Macau Government—FDCT, in 2014 and 2018. He is currently a Technical Program Committee Member of ISSCC and a Distinguished Lecturer of the IEEE CASS.

HADI HEIDARI (Senior Member, IEEE) is currently an Associate Professor (Senior Lecturer) with the James Watt School of Engineering and also the Head of the Microelectronics Lab (meLAB: www.melabresearch.com), University of Glasgow, U.K. He has authored more than 100 articles in top-tier peer reviewed journals and international conferences. He was a member of the IEEE Circuits and Systems Society Board of Governors, from 2018 to 2020, the IEEE Sensors Council Member-at-Large from 2020 to 2021, and a Fellow of the Higher Education Academy (FHEA). He has been the recipient of a number of awards including the 2019 IEEE Sensors Council Young Professional Award, the Rewards for Excellence prize from the University of Glasgow, in 2018, the IEEE CASS Scholarship (NGCAS'17 conference), Silk Road Award from the Solid-State Circuits Conference (ISSCC'16), Best Paper Award from the IEEE ISCAS'14 Conference, and the Gold Leaf Award from the IEEE PRIME'14 Conference. He is the General Chair of 27th IEEE ICECS 2020 and the Technical Program Chair of IEEE PRIME'19, and serves on the organizing committee for several conferences including the UK Circuits and Systems Workshop (UKCAS), UK-China Emerging Technologies (UCET) Conference, IEEE SENSORS'16 and '17, NGCAS'17, BioCAS'18, PRIME'15, ISCAS'23, and the organizer of several special sessions on the IEEE Conferences. His research has been funded by major research councils and funding organizations including the European Commission, EPSRC, Royal Society, and Scottish Funding Council. He is part of the €8.4M EU H2020 FET-Proactive project on ''Hybrid Enhanced Regenerative Medicine Systems (HERMES)''. He is an Associate Editor for the IEEE JOURNAL OF ELECTROMAGNETICS, *RF and Microwaves in Medicine and Biology*, and IEEE ACCESS, an Editor of *Microelectronics Journal* (ELSEVIER), and a Guest Editor for the IEEE SENSORS JOURNAL, and *Frontiers in Neuroscience*. He has a grant portfolio of £1 million funded by major research councils and funding organizations including European Commission, UK's EPSRC, Royal Society, Royal Academy of Engineering, and Scottish Funding Council.

SAMEH O. ABDELLATIF (Senior Member, IEEE) received the B.S. degree in electronics and communication from Ain Shams University, Cairo, Egypt, in 2009, the M.Sc. degree in semiconductor nano-structures from Ain Shams University, Cairo, Egypt, in 2012, and the Ph.D. degree from the University of Duisburg-Essen is dealing with Mesoporous based solar cells. He is currently a Lecturer with the Electrical Engineering Department, The British University in Egypt (BUE), where he is also a Researcher with the Centre of Emerging Learning Technology (CELT). In addition, he is also a Guest Researcher with the Max-Planck-Institut für Kohlenforschung, Mülheim, Germany.

MUHAMMAD ALI IMRAN (Senior Member, IEEE) is currently a Professor of wireless communication systems with research interests in self-organized networks, wireless networked control systems, and the wireless sensor systems. He also heads the Communications, Sensing and Imaging CSI Research Group, University of Glasgow. He is also an Affiliate Professor with The University of Oklahoma, USA, and also a Visiting Professor with the 5G Innovation Centre, University of Surrey, U.K. He has more than 18 years of combined academic and industry experience with several leading roles in multi-million pounds funded projects. He has been awarded 15 patents. He has authored or coauthored more than 400 journal and conference publications. He was an editor of two books and authored more than 15 book chapters. He has successfully supervised more than 40 master's students at Ph.D. level. He has been a consultant to international projects and local companies in the area of self-organized networks. He is a Fellow of IET and a Senior Fellow of HEA.

RAMI GHANNAM (Senior Member, IEEE) received the B.Eng. degree in electronic engineering from King's College, the D.I.C. and M.Sc. degrees from Imperial College London, and the Ph.D. degree from the University of Cambridge, in 2007. He held previous industrial positions with Nortel Networks and IBM Research GmbH. He is currently a Lecturer (Assistant Professor) of electronic and nanoscale engineering with the University of Glasgow. His research interests include energy harvesters and engineering education. He is a Senior Fellow of Glasgow's RET Scheme. He received the Siemens Prize for his B.Eng. degree. He serves as Scotland's Regional Chair for the IEEE Education Society. He is also an Associate Editor of the IEEE TRANSACTIONS ON ENGINEERING EDUCATION and IEEE ACCESS.